INTERNATIONAL JOURNAL FOR NUMERICAL METHODS IN ENGINEERING
Int. J. Numer. Meth. Engng. **43**, 365–388 (1998)

DYNAMIC AND STATIC ANALYSIS OF CRACKS USING THE HYPERSINGULAR FORMULATION OF THE BOUNDARY ELEMENT METHOD

FRANCISCO CHIRINO[1] AND RAMÓN ABASCAL[2,*]

[1] *Escuela Técnica Superior de Ingenieros Industriales, Las Palmas de Gran Canaria, Spain*
[2] *Escuela Superior de Ingenieros, Camino de los Descubrimientos s/n, E-41092 - Sevilla, Spain*

ABSTRACT

A new methodology for computing dynamic stress intensity factors in the frequency domain based on the mixed boundary element method, a combination of the equations corresponding to the integral representations of displacements and tractions, is proposed and analysed. The expressions of hypersingular fundamental solution are presented and their singular parts extracted. Also, a discontinuous *Singular-Quarter-Point* element is constructed. Finally, various parametric computations and applications are described in order to illustrate the simplicity and accuracy of the proposed method as applied to both static and dynamic problems. © 1998 John Wiley & Sons, Ltd.

KEY WORDS: stress intensity factor; hypersingular formulation; fracture mechanics; mixed boundary element method; dynamics

1. INTRODUCTION

The determination of static and dynamic *Stress Intensity Factors* (*SIFs*) is of a high current interest in Fracture Mechanics. Much theoretical and numerical research effort has been aimed in this direction. Numerical investigations have led to various approaches largely based on the *Finite Element Method* (*FEM*) and the *Boundary Element Method* (*BEM*), two effective, powerful choices for analysing this type of problem.

The *BEM*, used in this work, is specially suitable for calculating *SIFs* in brittle materials that exhibit a linear behaviour; there is a wealth of literature on this topic (e.g. References 1–3).

The development of elements with specific shape functions that allow a efficient approximation for the displacements and tractions near the crack tip (e.g. *Quarter-Point* (*QP*) and *Singular-Quarter-Point* (*SQP*) elements), has considerably facilitated the use of the *BEM* for calculating *SIFs*. The earliest elements of this type for use with the *BEM* in addressing static problems were developed by Martinez *et al.*[4] based on previous *FEM* developments but incorporating the singular representation of tractions. Subsequently, they were used by Chirino *et al.*[5] to solve dynamic problems in the frequency domain, and by Dominguez *et al.*,[6] to address transient problems. These elements have also been used in the Dual Reciprocity Method by Chirino *et al.*[7] to compare the results for various transient problems.

* Correspondence to: Ramón Abascal, Escuela Superior de Ingenieros, Camino de los Descubrimientos s/n, E-41092 - Sevilla, Spain. E-mail: abascal@cica.es
Contract/grant sponsor: DGICYT; Contract/grant number: PB 93-1184; Contract/grant number: PB 93-1191

CCC 0029–5981/98/020365–24$17.50

Received 15 April 1997
Revised 16 December 1997

Recent breakthroughs in hypersingular formulations have enabled the development of new applications for the *BEM*. Thus, Sáez *et al.*[8] calculated *SIFs* for static problems by using a mixed formulation similar to that previously reported by Portela *et al.*[9] and developed a discontinuous hypersingular *QP* element that allows the problem to be modelled with the need for no *SQP* elements. This mixed technique involves using the integral representation for displacements at one crack edge and that for tractions (a hypersingular formulation) at the other. In this way, similar (but unequal) equations are produced for each pair of collocation points along the crack that allow the problem to be solved; also, because the discontinuous elements used include a collocation point very near the crack tip, the corresponding *SIF* can be computed highly accurately from its displacements (i.e. the crack opening), without the knowledge of internal stresses in the material, which are indispensable for virtually all existing formulations.

This mixed method, also termed *dual* because it uses two integral representations simultaneously, was recently used by Fedelinski *et al.* to solve transient dynamic problems, both directly[10] and by use of the Laplace transform.[11] In the latter case, a solution similar to that obtained herein was reported after the present work was finished.

This paper reports a hypersingular formulation for two-dimensional dynamic problems in the frequency domain, a study of this fundamental solution by splitting nuclei into their singular and non-singular parts, and present a discontinuous hypersingular *SQP* element to obtain the *SIFs* for cracks in brittle materials (this element should be specially useful when the crack occurs along an interface between two parts of the model, as well as in propagation problems). Application of the proposed formulation is illustrated by parametric studies of static and dynamic problems, deriving suitability criteria and showing his ease use and accuracy.

2. INTEGRAL REPRESENTATION OF DISPLACEMENTS

Displacements at a point $\boldsymbol{\xi}$ in a domain Ω corresponding to a harmonic problem can be represented in integral form at each frequency ω by

$$c_{ik}(\boldsymbol{\xi})u_k(\boldsymbol{\xi};\omega) + \int_\Gamma p^*_{ik}(\mathbf{x},\boldsymbol{\xi};\omega)\, u_k(\mathbf{x};\omega)\, \mathrm{d}\Gamma(\mathbf{x}) = \int_\Gamma u^*_{ik}(\mathbf{x},\boldsymbol{\xi};\omega)\, p_k(\mathbf{x};\omega)\, \mathrm{d}\Gamma(\mathbf{x}) \tag{1}$$

provided body forces are zero.

The previous equation must be integrated in terms of the Cauchy principal value; $u_k(\mathbf{x};\omega)$ and $p_k(\mathbf{x};\omega)$ are the k components of the displacements and tractions, respectively, at any point $\mathbf{x}$ in the boundary at frequency ω; $c_{ik}(\boldsymbol{\xi}) = \delta_{ik}$ if point $\boldsymbol{\xi}$ is inside domain Ω, $c_{ik}(\boldsymbol{\xi}) = 1/2\,\delta_{ik}$ if $\boldsymbol{\xi}$ belongs to the boundary (and this is smooth), and $c_{ik}(\boldsymbol{\xi}) = 0$ if $\boldsymbol{\xi}$ is outside the domain.

Functions $p^*_{ik}(\mathbf{x},\boldsymbol{\xi};\omega)$ and $u^*_{ik}(\mathbf{x},\boldsymbol{\xi};\omega)$ are the fundamental solutions to the elastic problem involving a harmonic point load of frequency ω located at point $\boldsymbol{\xi}$ in direction i; for the two-dimensional case, they can be expressed as

$$u^*_{ik}(\mathbf{x},\boldsymbol{\xi};\omega) = \frac{1}{2\pi\mu}[\psi\,\delta_{ik} - \chi r_{,i} r_{,k}] \tag{2}$$

$$\begin{aligned} p^*_{ik}(\mathbf{x},\boldsymbol{\xi};\omega) = \frac{1}{2\pi}\Bigg[& \left(\frac{\partial\psi}{\partial r} - \frac{\chi}{r}\right)\left(\delta_{ik}\frac{\partial r}{\partial \eta} + r_{,k}\eta_i\right) - 2\frac{\chi}{r}\left(r_{,i}\eta_k - 2r_{,i}r_{,k}\frac{\partial r}{\partial \eta}\right) \\ & -2\frac{\partial\chi}{\partial r} r_{,i} r_{,k}\frac{\partial r}{\partial \eta} + \left(\frac{c_p^2}{c_s^2} - 2\right)\left(\frac{\partial\psi}{\partial r} - \frac{\partial\chi}{\partial r} - \frac{\chi}{r}\right) r_{,i}\eta_k\Bigg] \end{aligned} \tag{3}$$

where ψ and χ are given by

$$\psi = K_0(z_s) + \frac{1}{z_s}\left[K_1(z_s) - \frac{c_s}{c_p}K_1(z_p)\right] \tag{4}$$

$$\chi = \left[K_0(z_s) + \frac{2}{z_s}K_1(z_s)\right] - \frac{c_s^2}{c_p^2}\left[K_0(z_p) + \frac{2}{z_p}K_1(z_p)\right] \tag{5}$$

$$z_s = \frac{\mathrm{i}\omega r}{c_s}; \qquad z_p = \frac{\mathrm{i}\omega r}{c_p}; \qquad \mathrm{i} = \sqrt{-1} \tag{6}$$

μ being the shear modulus; c_s and c_p the velocities of waves S and P, respectively; $r = |\mathbf{x} - \boldsymbol{\xi}|$ the vector radius between the point of load application $\boldsymbol{\xi}$ and the calculation point $\mathbf{x}$; $r_{,i}$ its derivative with respect to co-ordinate x_i; η_k component k of the normal to the boundary at point $\mathbf{x}$; and $K_\alpha(z)$ modified Bessel functions that can be expanded when $z \to 0$ as

$$K_0(z) = f_0(z) + \sum_{k=1}^{\infty}\left[f_0(z) + \sum_{n=1}^{n=k}\frac{1}{n}\right]\frac{1}{(k!)^2}\left(\frac{z}{2}\right)^{2k} \tag{7}$$

$$K_1(z) = f_1(z) - \sum_{k=1}^{\infty}\left[f_0(z) + \frac{1}{2(k+1)} + \sum_{n=1}^{n=k}\frac{1}{n}\right]\frac{1}{k!(k+1)!}\left(\frac{z}{2}\right)^{2k} \tag{8}$$

the initial terms of which are

$$f_0(z) = -\ln\frac{z}{2} - \gamma, \qquad f_1(z) = \frac{1}{z} - \frac{z}{2}\left(f_0(z) + \frac{1}{2}\right) \tag{9}$$

where γ is the Euler constant.

Under static conditions, the fundamental solution becomes

$$u_{ik}^*)_{\text{static}} = \frac{1}{8\pi\mu(1-\nu)}\left[(3-4\nu)\ln\left(\frac{1}{r}\right)\delta_{ik} + r_{,i}r_{,k}\right] \tag{10}$$

$$p_{ik}^*)_{\text{static}} = -\frac{1}{4\pi(1-\nu)}\frac{1}{r}\left[\frac{\partial r}{\partial \eta}((1-2\nu)\delta_{ik} + 2r_{,i}r_{,k}) - (1-2\nu)(r_{,i}\eta_k - r_{,k}\eta_i)\right] \tag{11}$$

ν being the Poisson modulus.

The numerical treatment for nuclei $u_{ik}^*(\mathbf{x}, \boldsymbol{\xi}; \omega)$ and $p_{ik}^*(\mathbf{x}, \boldsymbol{\xi}; \omega)$ has been studied by several authors; one of the most effective procedures (prominent among which is that reported by Dominguez[1]) involves splitting them into their singular and non-singular parts, particularly with a view to their integration.

3. INTEGRAL REPRESENTATION OF TRACTIONS

The integral representation of tractions in a harmonic problem can be calculated by derivation of the integral representation of displacements at a point $\boldsymbol{\xi}$ inside domain Ω, equation (1), calculation

of the stress tensor $\sigma_{ij}(\boldsymbol{\xi})$ from such derivatives by using Hooke's law, and determination of the tractions referred to the normal $N_j(\boldsymbol{\xi})$. The procedure is completed by a limiting process that allows matrix $\hat{c}_{ik}(\boldsymbol{\xi})$ to be calculated. In this way, the following integral representation for tractions at each frequency ω is obtained

$$\hat{c}_{ik}(\boldsymbol{\xi})\, p_k(\boldsymbol{\xi};\omega) + N_j(\boldsymbol{\xi}) \oint_{\Gamma} s^*_{ijk}(\mathbf{x},\boldsymbol{\xi};\omega)\, u_k(\mathbf{x};\omega)\, \mathrm{d}\Gamma(\mathbf{x})$$
$$= N_j(\boldsymbol{\xi}) \oint_{\Gamma} d^*_{ijk}(\mathbf{x},\boldsymbol{\xi};\omega)\, p_k(\mathbf{x};\omega)\, \mathrm{d}\Gamma(\mathbf{x}) \tag{12}$$

where, again, zero body forces are assumed.

The integral on the left-hand side of equation (12) must be interpreted as a Hadamard Finite Part Integral and that on the right-hand side as a Cauchy Principal Value; also, nuclei $d^*_{ijk}(\mathbf{x},\xi;\omega)$ and $s^*_{ijk}(\mathbf{x},\boldsymbol{\xi};\omega)$ are linear combinations of the derivatives of $u^*_{ik}(\mathbf{x},\boldsymbol{\xi};\omega)$ and $p^*_{ik}(\mathbf{x},\boldsymbol{\xi};\omega)$, respectively. Finally, $\hat{c}_{ik}(\boldsymbol{\xi}) = \delta_{ik}$ if point $\boldsymbol{\xi}$ is inside domain Ω, $\hat{c}_{ik}(\boldsymbol{\xi}) = 1/2\,\delta_{ik}$ if $\boldsymbol{\xi}$ belongs to the boundary (and this is smooth), and $\hat{c}_{ik}(\boldsymbol{\xi}) = 0$ if $\boldsymbol{\xi}$ is outside the domain.

The interpretation as Hadamard Finite Part Integral constrains the numerical formulation because it imposes the conditions that the displacement function must be differentiable at the collocation point and that its first derivative must fulfill the Hölder condition, $u_k(\boldsymbol{\xi};\omega) \in C^1$, which inevitably entails choosing collocation points inside the element.

It should also be noted that the integral representation of tractions at a non-smooth point of the boundary cannot be obtained as the sole function of displacements and tractions along the boundary by using a limiting process from an internal point; rather, the limiting process must be applied to their derivatives and, subsequently, the integral representation of tractions calculated.

Based on the properties of the nuclei involved, this solution is usually named *hypersingular*. Let us now analyse the expressions for the nuclei.

The expression for nucleus $d^*_{ijk}(\mathbf{x},\boldsymbol{\xi};\omega)$ in two-dimensional problems is

$$d^*_{ijk}(\mathbf{x},\boldsymbol{\xi};\omega) = \lambda\delta_{ij}\, u^*_{mk,m} + \mu(u^*_{ik,j} + u^*_{jk,i}) \tag{13}$$

substitution of u^*_{ij} into which yields

$$d^*_{ijk}(\mathbf{x},\boldsymbol{\xi};\omega) = -\frac{1}{2\pi}\frac{\partial\psi}{\partial r}\left[\frac{\lambda}{\mu}\delta_{ij}r_{,k} + (\delta_{ik}r_{,j} + \delta_{jk}r_{,i})\right]$$
$$+\frac{1}{2\pi}\frac{\partial\chi}{\partial r}\left[\frac{\lambda}{\mu}\delta_{ij}r_{,k} + 2r_{,i}r_{,j}r_{,k}\right]$$
$$+\frac{1}{2\pi}\frac{\chi}{r}\left[\frac{\lambda}{\mu}\delta_{ij}r_{,k} + (2\delta_{ij}r_{,k} + \delta_{ik}r_{,j} + \delta_{jk}r_{,i} - 4r_{,i}r_{,j}r_{,k})\right] \tag{14}$$

where λ is the Lame constant

$$\lambda = \frac{2\upsilon}{1-2\upsilon}\mu \tag{15}$$

The corresponding expression for a static problem is

$$d^*_{ijk})_{\text{static}} = \frac{1}{4\pi(1-\upsilon)}\frac{1}{r}[(1-2\upsilon)(\delta_{jk}r_{,i} + \delta_{ik}r_{,j} - \delta_{ij}r_{,k}) + 2r_{,i}r_{,j}r_{,k}] \tag{16}$$

By analogy with this last, the nucleus corresponding to the dynamic problem can be expressed as follows:

$$d^*_{ijk}(\mathbf{x}, \xi; \omega) = Q_1 \delta_{ij} r_{,k} + Q_2 \delta_{ik} r_{,j} + Q_3 \delta_{jk} r_{,i} + Q_4 r_{,i} r_{,j} r_{,k} \tag{17}$$

where

$$Q_1 = \frac{1}{2\pi} \left[\left(-\frac{\partial \psi}{\partial r} + \frac{\partial \chi}{\partial r} + \frac{\chi}{r} \right) \frac{\lambda}{\mu} + \frac{2\chi}{r} \right] \tag{18}$$

$$Q_2 = Q_3 = \frac{1}{2\pi} \left[-\frac{\partial \psi}{\partial r} + \frac{\chi}{r} \right] \tag{19}$$

$$Q_4 = \frac{1}{\pi} \left[\frac{\partial \chi}{\partial r} - 2\frac{\chi}{r} \right] \tag{20}$$

with

$$\frac{\lambda}{\mu} = \frac{c_p^2}{c_s^2} - 2 \tag{21}$$

The singular part is derived by determining the singularities in the terms that appear in functions Q_i in substituting functions $f_0(z)$ and $f_1(z)$ corresponding to the initial part of the expansions of the Bessel functions. Thus, the dynamic solution can be expressed as

$$d^*_{ijk}(\mathbf{x}, \boldsymbol{\xi}; \omega) = d^*_{ijk})_{\text{sing}} + d^*_{ijk})_{\text{nonsing}} \tag{22}$$

the singular part being

$$d^*_{ijk})_{\text{sing}} = Q_1)_{\text{sing}} \delta_{ij} r_{,k} + Q_2)_{\text{sing}} \delta_{ik} r_{,j} + Q_3)_{\text{sing}} \delta_{jk} r_{,i} + Q_4)_{\text{sing}} r_{,i} r_{,j} r_{,k} \tag{23}$$

where

$$Q_1)_{\text{sing}} = \frac{1}{4\pi r} \left[-\frac{1-2\upsilon}{(1-\upsilon)} - \left(1 - 2\frac{c_s^2}{c_p^2} \right) z_p^2 \left(f_0(z_p) + \frac{1}{2} \right) \right] \tag{24}$$

$$Q_2)_{\text{sing}} = Q_3)_{\text{sing}} = \frac{1}{4\pi r} \left[\frac{1-2\upsilon}{(1-\upsilon)} - z_s^2 \left(f_0(z_s) + \frac{1}{2} \right) \right] \tag{25}$$

$$Q_4)_{\text{sing}} = \frac{1}{4\pi r} \left[\frac{2}{(1-\upsilon)} + 2z_s^2 \left(f_0(z_s) + \frac{1}{2} \right) - 2\frac{c_s^2}{c_p^2} z_p^2 \left(f_0(z_p) + \frac{1}{2} \right) \right] \tag{26}$$

so

$$d^*_{ijk})_{\text{sing}} = d^*_{ijk})_{\text{static}} + d^*_{ijk})_{\text{additional}} \tag{27}$$

and

$$\lim_{z_s \to 0,\, z_p \to 0} [d^*_{ijk})_{\text{additional}}] = 0 \tag{28}$$

i.e. when $r \to 0$ or $\omega \to 0$, the nucleus of the dynamic problem tends to that of the static problem, so the singular integrals for both nuclei are identical and can be operated similarly in the numeric formulation.

The expression for nucleus $s^*_{ijk}(\mathbf{x},\boldsymbol{\xi};\omega)$ in the two-dimensional case can be written as

$$s^*_{ijk}(\mathbf{x},\boldsymbol{\xi};\omega)=\lambda\delta_{ij}\,p^*_{mk,m}+\mu(p^*_{ik,j}+p^*_{jk,i}) \tag{29}$$

where $p^*_{ij,k}$ is given by

$$\begin{aligned}
p^*_{ij,k} = &-\frac{1}{2\pi}\frac{\partial^2\psi}{\partial r^2}\left[\frac{\lambda}{\mu}r_{,i}r_{,k}\eta_j+\left(\delta_{ij}\frac{\partial r}{\partial\eta}r_{,k}+\eta_i r_{,j}r_{,k}\right)\right]\\
&-\frac{1}{2\pi}\frac{1}{r}\frac{\partial\psi}{\partial r}\left[\frac{\lambda}{\mu}(\eta_j\delta_{ik}-\eta_j r_{,i}r_{,k})+(\delta_{jk}\eta_i+\delta_{ij}\eta_k)\right.\\
&\left.-\left(\delta_{ij}r_{,k}\frac{\partial r}{\partial\eta}+\eta_i r_{,j}r_{,k}\right)\right]+\frac{1}{2\pi}\frac{\partial^2\chi}{\partial r^2}\left[\frac{\lambda}{\mu}r_{,i}r_{,k}\eta_j+2\frac{\partial r}{\partial\eta}r_{,i}r_{,j}r_{,k}\right]\\
&+\frac{1}{2\pi}\frac{1}{r}\frac{\partial\chi}{\partial r}\left[\frac{\lambda}{\mu}\eta_j\delta_{ik}+\left(2r_{,i}r_{,k}\eta_j+\delta_{ij}r_{,k}\frac{\partial r}{\partial\eta}+2\delta_{jk}r_{,i}\frac{\partial r}{\partial\eta}\right)\right.\\
&\left.+\left(2\delta_{ik}r_{,j}\frac{\partial r}{\partial\eta}-10r_{,i}r_{,j}r_{,k}\frac{\partial r}{\partial\eta}+\eta_i r_{,j}r_{,k}+2r_{,i}r_{,j}\eta_k\right)\right]\\
&-\frac{1}{2\pi}\frac{\chi}{r^2}\left[\frac{\lambda}{\mu}(2r_{,i}r_{,k}\eta_j-\delta_{ik}\eta_j)+2\eta_j(-\delta_{ik}+2r_{,i}r_{,k})\right.\\
&+\left(\eta_i(-\delta_{jk}+2r_{,j}r_{,k})+\delta_{ij}\left(-\eta_k+2r_{,k}\frac{\partial r}{\partial\eta}\right)-16r_{,i}r_{,j}r_{,k}\frac{\partial r}{\partial\eta}\right)\\
&\left.+\left(4\delta_{ik}r_{,j}\frac{\partial r}{\partial\eta}+4\delta_{jk}r_{,i}\frac{\partial r}{\partial\eta}+4r_{,i}r_{,j}\eta_k\right)\right]
\end{aligned} \tag{30}$$

substitution of which yields

$$\begin{aligned}
s^*_{ijk}(\mathbf{x},\xi;\omega) = &P_1\frac{\partial r}{\partial\eta}\delta_{ij}r_{,k}+P_2\frac{\partial r}{\partial\eta}(\delta_{ik}r_{,j}+\delta_{jk}r_{,i})\\
&+P_3\frac{\partial r}{\partial\eta}r_{,i}r_{,j}r_{,k}+P_4(r_{,i}r_{,k}\eta_j+r_{,j}r_{,k}\eta_i)\\
&+P_5 r_{,i}r_{,j}\eta_k+P_6(\delta_{ik}\eta_j+\delta_{jk}\eta_i)+P_7\delta_{ij}\eta_k
\end{aligned} \tag{31}$$

with

$$P_1=P_5=\frac{\lambda}{\pi}\left(-\frac{\partial^2\psi}{\partial r^2}+\frac{1}{r}\frac{\partial\psi}{\partial r}+\frac{\partial^2\chi}{\partial r^2}-2\frac{\chi}{r^2}\right)+\frac{2\mu}{\pi r}\left(\frac{\partial\chi}{\partial r}-2\frac{\chi}{r}\right) \tag{32}$$

$$P_2=P_4=\frac{\mu}{2\pi}\left(-\frac{\partial^2\psi}{\partial r^2}+\frac{1}{r}\frac{\partial\psi}{\partial r}+3\frac{1}{r}\frac{\partial\chi}{\partial r}-6\frac{\chi}{r^2}\right) \tag{33}$$

$$P_3=\frac{2\mu}{\pi}\left(\frac{\partial^2\chi}{\partial r^2}-5\frac{1}{r}\frac{\partial\chi}{\partial r}+8\frac{\chi}{r^2}\right) \tag{34}$$

$$P_6=\frac{\mu}{\pi r}\left(-\frac{\partial\psi}{\partial r}+\frac{\chi}{r}\right) \tag{35}$$

$$P_7 = \frac{\lambda^2}{2\pi\mu}\left(-\frac{\partial^2\psi}{\partial r^2} - \frac{1}{r}\frac{\partial\psi}{\partial r} + \frac{\partial^2\chi}{\partial r^2} + 2\frac{1}{r}\frac{\partial\chi}{\partial r}\right) + \frac{2\lambda}{\pi r}\left(-\frac{\partial\psi}{\partial r} + \frac{\partial\chi}{\partial r} + \frac{\chi}{r}\right) + \frac{2\mu}{\pi}\frac{\chi}{r^2} \tag{36}$$

for the dynamic case and

$$s^*_{ijk})_{\text{static}} = \frac{\mu}{2\pi(1-\nu)}\frac{1}{r^2}\left[2\frac{\partial r}{\partial\eta}((1-2\nu)\delta_{ij}r_{,k} + \nu(\delta_{ik}r_{,j} + \delta_{jk}r_{,i}) - 4r_{,i}r_{,j}r_{,k}) + 2\nu(r_{,i}r_{,k}\eta_j + r_{,j}r_{,k}\eta_i) + (1-2\nu)(2r_{,i}r_{,j}\eta_k + \delta_{ik}\eta_j + \delta_{jk}\eta_i) - (1-4\nu)\delta_{ij}\eta_k\right] \tag{37}$$

for the static case.

Similarly, one can write

$$s^*_{ijk}(\mathbf{x},\boldsymbol{\xi};\omega) = s^*_{ijk})_{\text{sing}} + s^*_{ijk})_{\text{nonsing}} \tag{38}$$

where the singular part of $s^*_{ijk}(\mathbf{x},\boldsymbol{\xi};\omega)$ can be obtained by the same procedure used with $d^*_{ijk}(\mathbf{x},\boldsymbol{\xi};\omega)$, using the first few terms in the Bessel function expansion

$$s^*_{ijk})_{\text{sing}} = P_1)_{\text{sing}}\frac{\partial r}{\partial\eta}\delta_{ij}r_{,k} + P_2)_{\text{sing}}\frac{\partial r}{\partial\eta}(\delta_{ik}r_{,j} + \delta_{jk}r_{,i}) + P_3)_{\text{sing}}\frac{\partial r}{\partial\eta}r_{,i}r_{,j}r_{,k} + P_4)_{\text{sing}}\frac{\partial r}{\partial\eta}(r_{,i}r_{,k}\eta_j + r_{,j}r_{,k}\eta_i) + P_5)_{\text{sing}}r_{,i}r_{,j}\eta_k + P_6)_{\text{sing}}(\delta_{ik}\eta_j + \delta_{jk}\eta_i) + P_7)_{\text{sing}}\delta_{ij}\eta_k \tag{39}$$

where

$$P_1)_{\text{sing}} = P_5)_{\text{sing}} = \frac{\mu}{\pi r^2}\left[\frac{(1-2\nu)}{(1-\nu)} - \frac{3}{2}\frac{c_s^2}{c_p^2}z_p^2 + \frac{(z_s^2+z_p^2)}{2} + z_s^2 f_0(z_s) - \frac{c_s^2}{c_p^2}z_p^2 f_0(z_p)\right] \tag{40}$$

$$P_2)_{\text{sing}} = P_4)_{\text{sing}} = \frac{\mu}{\pi r^2}\left[\frac{\nu}{(1-\nu)} - \frac{1}{2}\frac{c_s^2}{c_p^2}z_p^2 + \frac{3}{4}z_s^2 + z_s^2 f_0(z_s) - \frac{c_s^2}{c_p^2}z_p^2 f_0(z_p)\right] \tag{41}$$

$$P_3)_{\text{sing}} = \frac{\mu}{\pi r^2}\left[-\frac{4}{(1-\nu)} + 4\frac{c_s^2}{c_p^2}z_p^2 - 4z_s^2 + 6\frac{c_s^2}{c_p^2}z_p^2 f_0(z_p) - 6z_s^2 f_0(z_s)\right] \tag{42}$$

$$P_6)_{\text{sing}} = \frac{\mu}{\pi r^2}\left[\frac{(1-2\nu)}{2(1-\nu)} - \frac{z_s^2}{2}\left(f_0(z_s) + \frac{1}{2}\right)\right] \tag{43}$$

$$P_7)_{\text{sing}} = \frac{\mu}{\pi r^2}\left[-\frac{(1-4\nu)}{2(1-\nu)} - z_p^2\left(\frac{1}{2} - \frac{c_p^2}{c_s^2}\right) + f_0(z_p)\left(z_p^2 - \frac{z_s^2}{2}\right)\right] \tag{44}$$

Also,

$$s^*_{ijk})_{\text{sing}} = s^*_{ijk})_{\text{static}} + s^*_{ijk})_{\text{additional}} \tag{45}$$

where

$$\lim_{z_s \to 0, z_p \to 0} [s^*_{ijk})_{\text{additional}}] = 0 \tag{46}$$

i.e. again, when $r \to 0$ or $\omega \to 0$, the nucleus of the dynamic problem tends to that of the static problem, so the singular integrals for both nuclei are identical and can be computed similarly.

4. DISCRETIZATION OF INTEGRAL REPRESENTATIONS

Discretization was done by using quadratic functions for the approximations to both the geometry and the displacements and tractions. Despite the similar approximations used, the nodes employed to approximate the geometry and the variables were not the same in every case.

The boundary geometry was approximated by using elements with two nodes at their ends, N1 and N3, and an intermediate node N2 (see Figure 1(a)), i.e.

$$x_k = x_k^1 \phi_{1G} + x_k^2 \phi_{2G} + x_k^3 \phi_{3G} \tag{47}$$

where x_k^m is co-ordinate x_k for node m and ϕ_{mG} its associated shape function

$$\phi_{1G} = -\tfrac{1}{2}\xi(1-\xi), \quad \phi_{2G} = (1-\xi^2), \quad \phi_{3G} = \tfrac{1}{2}\xi(1+\xi) \tag{48}$$

ξ being the dimensionless co-ordinate ($\xi = -1$ at node N1, $\xi = 0$ at node N2 and $\xi = 1$ at node N3).

Displacements and tractions at the boundary will be approximated from their values at the collocation points (NC1, NC2 and NC3 in Figure 1(b)), which, as a rule, will not coincide with those used to represent the geometry. If NC1 and NC3 are located at the ends of the element, then the interelemental continuity condition will be fulfilled and the two will be continuous elements; on the other hand, if the nodes are internal the elements will be discontinuous.

The variables are thus approximated with the following expressions

$$u_k = u_k^1 \phi_1 + u_k^2 \phi_2 + u_k^3 \phi_3 \tag{49}$$

$$p_k = p_k^1 \phi_1 + p_k^2 \phi_2 + p_k^3 \phi_3 \tag{50}$$

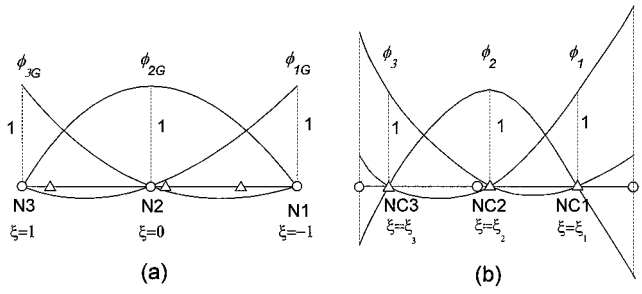

Figure 1. Shape functions used to represent the geometry and variables

where u_k^m and p_k^m are the displacements and tractions in direction k at collocation point m, and ϕ_m is the shape function associated to that point

$$\phi_1 = \frac{(\xi - \xi_2)(\xi - \xi_3)}{(\xi_1 - \xi_2)(\xi_1 - \xi_3)}, \quad \phi_2 = \frac{(\xi - \xi_1)(\xi - \xi_3)}{(\xi_2 - \xi_1)(\xi_2 - \xi_3)}, \quad \phi_3 = \frac{(\xi - \xi_1)(\xi - \xi_2)}{(\xi_3 - \xi_1)(\xi_3 - \xi_2)} \tag{51}$$

ξ_m denoting the natural co-ordinate associated to collocation point m.

The use of discontinuous elements is mandatory in order to discretize the integral representation of tractions because the first derivative must exist and fulfill the Hölder condition; on the other hand, the integral representation of displacements can be implemented using continuous or discontinuous elements indifferently.

Based on this approach, the displacements and tractions of the quadratic element can be expressed in matrix form as

$$\mathbf{u} = \begin{Bmatrix} u_1 \\ u_2 \end{Bmatrix} = \begin{bmatrix} \phi_1 & 0 & \phi_2 & 0 & \phi_3 & 0 \\ 0 & \phi_1 & 0 & \phi_2 & 0 & \phi_3 \end{bmatrix} \begin{Bmatrix} u_1^1 \\ u_2^1 \\ u_1^2 \\ u_2^2 \\ u_1^3 \\ u_2^3 \end{Bmatrix}^j = \mathbf{\Phi} \mathbf{u}^j \tag{52}$$

$$\mathbf{p} = \begin{Bmatrix} p_1 \\ p_2 \end{Bmatrix} = \begin{bmatrix} \phi_1 & 0 & \phi_2 & 0 & \phi_3 & 0 \\ 0 & \phi_1 & 0 & \phi_2 & 0 & \phi_3 \end{bmatrix} \begin{Bmatrix} p_1^1 \\ p_2^1 \\ p_1^2 \\ p_2^2 \\ p_1^3 \\ p_2^3 \end{Bmatrix}^j = \mathbf{\Phi} \mathbf{p}^j \tag{53}$$

substitution of which into the discretized integral representations yields

$$\mathbf{c}^i \mathbf{u}^i + \sum_{j=1}^{NE} \left[\oint_{\Gamma j} \mathbf{p}^* \mathbf{\Phi} \, \mathrm{d}\Gamma \right] \mathbf{u}^j = \sum_{j=1}^{NE} \left[\oint_{\Gamma j} \mathbf{u}^* \mathbf{\Phi} \, \mathrm{d}\Gamma \right] \mathbf{p}^j \tag{54}$$

$$\hat{\mathbf{c}}^i \mathbf{p}^i + \sum_{j=1}^{NE} \left[\neq \int_{\Gamma j} \mathbf{s}^* \mathbf{N} \mathbf{\Phi} \, \mathrm{d}\Gamma \right] \mathbf{u}^j = \sum_{j=1}^{NE} \left[\oint_{\Gamma j} \mathbf{d}^* \mathbf{N} \mathbf{\Phi} \, \mathrm{d}\Gamma \right] \mathbf{p}^j \tag{55}$$

These equations can be used with any collocation point in such a way that, if as many equations as displacements or tractions are defined for all the collocation points, an equation system of the

type

$$\mathbf{Hu} = \mathbf{Gp} \tag{56}$$

is obtained that allows the system to be solved after boundary conditions are imposed.

5. QUARTER-POINT AND SINGULAR-QUARTER-POINT ELEMENTS

On the assumption of a linear elastic behaviour, stresses and displacements near a crack tip can be approximated by the following equation[12]

$$\sigma = a_0 \frac{1}{\sqrt{\bar{r}}} + a_1 + a_2\sqrt{\bar{r}} + \cdots \tag{57}$$

$$u = b_0 + b_1\sqrt{\bar{r}} + b_2\bar{r} + \cdots \tag{58}$$

where $\bar{r}$ is the distance from the crack tip to the point considered.

In order to characterize this behaviour, we shall used two types of elements for which special shape functions will be defined. One will be used to represent the portion of the crack edge near the tip and the other will be used at an internal boundary, thereby splitting the body into two parts (Figure 2).

The former case simply entails representing the behaviour of displacements because tractions are known. It suffices to place the central node of the element, whether continuous or discontinuous, at one-quarter of the element length on the side of the crack tip. It can readily be checked that, if the element is rectilinear, L its length, $\bar{r}$ the distance from the crack tip to any point of the element and $\xi = \xi_0 = \pm 1$ the natural co-ordinate of the crack tip, then equation (47) can be solved for ξ as follows:

$$\xi = \xi_0 \left(1 - 2\sqrt{\frac{\bar{r}}{L}} \right) \tag{59}$$

substitution of which into the expression for displacements, equation (49), yields

$$u_k = \alpha_k + \beta_k \sqrt{\frac{\bar{r}}{L}} + \delta_k \frac{\bar{r}}{L} \tag{60}$$

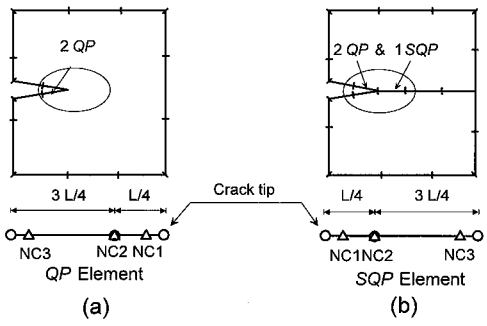

Figure 2. Use of *Quarter-Point* and *Singular-Quarter-Point* elements

This equation is of the same form as the theoretical expression, equation (58). Parameters α_k, β_k and δ_k, depend on the position of the collocation points in the boundary element and on the nodal values of the displacements in such a way that, if $\xi_2 = 0$ (i.e. if N2 and NC2 coincide, which will henceforward be assumed), then

$$\alpha_k = \frac{1-\xi_0\xi_3}{\xi_1(\xi_1-\xi_3)}u_k^1 + \frac{(\xi_0-\xi_3)(\xi_0-\xi_1)}{\xi_3\xi_1}u_k^2 - \frac{1-\xi_0\xi_1}{(\xi_1-\xi_3)\xi_3}u_k^3 \tag{61}$$

$$\beta_k = -\frac{2(2-\xi_0\xi_3)}{\xi_1(\xi_1-\xi_3)}u_k^1 - \frac{2(2-\xi_0\xi_1-\xi_0\xi_3)}{\xi_3\xi_1}u_k^2 + \frac{2(2-\xi_0\xi_1)}{(\xi_1-\xi_3)\xi_3}u_k^3 \tag{62}$$

$$\delta_k = \frac{4}{\xi_1(\xi_1-\xi_3)}u_k^1 + \frac{4}{\xi_3\xi_1}u_k^2 - \frac{4}{(\xi_1-\xi_3)\xi_3}u_k^3 \tag{63}$$

In this way, a representation of displacements similar to that near the crack is obtained. This element is usually referred to as a *Quarter-Point* (*QP*) element on account of the positions of the central node. The approximation of tractions is similar to that given by equation (60) except that, because nodal values are known, it does not condition the result.

The second element is of the *Singular-Quarter-Point* (*SQP*) type and allows one to represent the behaviour of not only the displacements, but also tractions near the crack tip. If, as previously, the element is assumed to be rectilinear and the central node is placed at one-quarter of its length to the crack tip, ξ and u_k can be expressed by means of equations (59) and (60), respectively. Then, taking advantage of the fact that the BEM approximates displacements and tractions separately, tractions are approximated in such a way that a behaviour similar to the theoretical one, equation (57), is obtained

$$p_k = \bar{p}_k^1\bar{\phi}_1 + \bar{p}_k^2\bar{\phi}_2 + \bar{p}_k^3\bar{\phi}_3 \tag{64}$$

where

$$\bar{\phi}_m = \phi_m\sqrt{\frac{L}{\bar{r}}} = \phi_m\frac{2\xi_0}{(\xi_0-\xi)}, \qquad \bar{p}_k^m = p_k^m\frac{(\xi_0-\xi_m)}{2\xi_0} \tag{65}$$

The singular denomination originates from the fact that the traction approximation function $\bar{\phi}_m$ possesses a singularity at the crack tip ($\xi = \xi_0$), that is of the same type as that of the stress field, equation (57).

The corresponding nodal parameter for a continuous element is taken to be the result of the following limit

$$\bar{p}_k^{1,3} = \lim_{\bar{r}\to 0}\left(p_k^{1,3}\sqrt{\frac{\bar{r}}{L}}\right) \tag{66}$$

6. CALCULATION OF STRESS INTENSITY FACTORS

The above described *QP* and *SQP* elements can be used in both integral representations, equations (1) and (12), and allow one to calculate *Stress Intensity Factors* (*SIFs*) easily and accurately.

The *SIFs* associated to modes I and II can be approximated via the stress tensor σ_{ij},[13] at the crack tip. If the crack runs in direction x_1, then the *SIFs* will be

$$K_{\mathrm{I}} = \lim_{\bar{r}\to 0}(\sigma_{22}\sqrt{2\pi\bar{r}}), \qquad K_{\mathrm{II}} = \lim_{\bar{r}\to 0}(\sigma_{12}\sqrt{2\pi\bar{r}}) \tag{67}$$

Other approximations can be obtained from the displacements

$$K_{\mathrm{I}} = \frac{\mu}{4(1-\nu)}\Delta u_2\sqrt{\frac{2\pi}{\bar{r}}}, \qquad K_{\mathrm{II}} = \frac{\mu}{4(1-\nu)}\Delta u_1\sqrt{\frac{2\pi}{\bar{r}}} \tag{68}$$

where Δu_1 and Δu_2 are the normal and shear relative displacements of the crack edges at a point near the crack tip.

The previous limits can be approximated by its values at any point near the crack tip. For a generic point with a natural co-ordinate ξ_i, the following expression holds

$$\lim_{\bar{r}\to 0}(\sigma_{k2}\sqrt{2\pi\bar{r}}) \simeq p_k(\xi_i)\sqrt{2\pi\,\bar{r}(\xi_i)} = \sqrt{2\pi L}\sum_{m=1}^{3}(\bar{p}_k^m\phi_m(\xi_i)) \tag{69}$$

Also, the crack opening at that point is given by

$$\Delta u_k\sqrt{\frac{2\pi}{\bar{r}}} = \Delta u_k(\xi_i)\sqrt{\frac{2\pi}{\bar{r}(\xi_i)}} = \sqrt{\frac{2\pi}{L}}\frac{2\xi_0}{(\xi_0-\xi_i)}\sum_{m=1}^{3}(\Delta u_k^m\phi_m(\xi_i)) \tag{70}$$

In this way, in the *SQP* element it can be associated a *SIF* value to each collocation point NCm as a function of nodal parameters $\bar{p}_k^m$

$$K_{\mathrm{I}}^{NCm} = \bar{p}_2^m\sqrt{2\pi L}, \qquad K_{\mathrm{II}}^{NCm} = \bar{p}_1^m\sqrt{2\pi L} \tag{71}$$

while for the *QP* element it can be associated to each point other *SIFs* values obtained from their crack openings

$$K_{\mathrm{I}}^{NCm} = \Delta u_2^m\frac{\mu}{2(1-\nu)}\frac{\xi_0}{(\xi_0-\xi_m)}\sqrt{\frac{2\pi}{L}}, \qquad K_{\mathrm{II}}^{NCm} = \Delta u_1^m\frac{\mu}{2(1-\nu)}\frac{\xi_0}{(\xi_0-\xi_m)}\sqrt{\frac{2\pi}{L}} \tag{72}$$

It can readily be checked that the most closely approximated values for *SIFs* are those obtained from the extrapolated values of stresses at the crack tip, $\xi_i = \xi_0$ in equation (69), and from the crack openings for the two collocations points located nearest to the tip, i.e. NC1 or NC2.

Similar approximations have been used by various authors in combination with the integral representation of displacements; prominent among them are those reported by Blandford *et al.*[14] and Martinez *et al.*[4] for static problems, Reference 5 for dynamic problems in the frequency domain, and Reference 6 for transient dynamic problems. They have also been used with the integral representation of tractions (the hypersingular fundamental solution) in static problems,[8] transient dynamic, both directly[10] and by use of the Laplace transform,[11] but only as regards the discontinuous *QP* element, never in relation to the discontinuous *SQP* element in static or dynamic problems.

7. EVALUATION OF INTEGRALS

Integrating the discretized expressions for the integral representations, equations (54) and (55), entails solving singular and hypersingular integrals if the collocation point belongs to the element that is being integrated; quasi-singular integrals when such an element is very near the collocation point; and non-singular integrals in other cases. We used a different procedure to solve each type of integral.

The singular and hypersingular integrations involved in the static problem were performed by using analytical procedures that provided specific expressions for each in the singular and hypersingular case provided the element geometry was rectilinear. In the dynamic problem, the integrals were solved by using an integration scheme involving splitting the nuclei into parts as reflected in equations (22), (27), (38) and (45) in such a way that singularities were concentrated in static nuclei, and using Gauss quadratures to solve the integrals for the additional and non-singular parts, both of which varied smoothly along the element. This nucleus splitting scheme is similar to that used by Dominguez[1] and Saez *et al.*,[8] to integrate the integral representation of displacements.

The quasi-singular integrals that are frequently encountered in using discontinuous elements have been resolved by numerical integration of the full expressions for the nuclei by splitting the integration interval as a function of the distance and using quadratures containing a fixed number of points in each sub-interval. This technique allows one to increase the number of integration points used near the singularity and to solve the integrals with adequate accuracy.

The integral from a distant point load was computed by using a quadrature containing a fixed number of points for all the elements.

The previous integration scheme is also applicable to *QP* elements, which are treated like any other type of element. *SQP* elements, however, entail distinguishing between those integrals that contain the displacement shape function, equation (60), which were computed by using the general procedure, and those that contain the singular shape functions, equation (64), for which specific expressions of their singular integrals were derived, while the general scheme was applied to the other types of integrals.

8. PARAMETRIC STUDIES AND NUMERICAL EXAMPLES

This section presents various parametric studies of static and dynamic problems intended to illustrate the degree of approximation achieved in computing *SIFs* on the basis of continuous and discontinuous *QP* and *SQP* elements, as well as to help one choose the most appropriate discretization for each individual problem. The different computation alternatives are compared; also, the effect of the discretization procedure on the results and the influence of the distance between the end nodes and the element tips, which will be assumed identical at both ends, are discussed.

The *SIFs* obtained from tractions extrapolated to the crack tip, equation (69) by using discontinuous *SQP* elements will henceforward be denoted by DET0, whereas those calculated from the displacements at the collocations points lying closest to the crack tip, NC1 and NC2, equation (72), by using discontinuous *QP* elements will be denoted by DEU1 and DEU2, respectively.

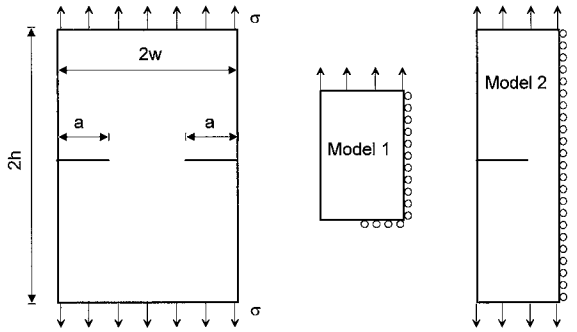

Figure 3. Rectangular sheet with two side cracks

8.1. Sheet with two side cracks. Static SIF

The first parametric study was conducted on a rectangular sheet (Figure 3) of dimensions $w = 3{\cdot}6$ cm and $h = 10{\cdot}8$ cm, with two side cracks of length $a = 1{\cdot}8$ cm, under a traction σ at both ends. The elasticity modulus to applied traction ratio was $E/\sigma = 5250{\cdot}0$, and the Poisson modulus $v = 0{\cdot}20$. The reference value adopted for the *SIF* value, 1·163, was taken from the nahdbook of Murakami,[15] which cites the paper of Nisitani[16] as its source, for $h/w = \infty$, with an estimated error of $\pm 0{\cdot}5$ per cent.

Parametric studies of static problems similar to this one were conducted in the continuous *SQP* element[4] and the discontinuous *QP* element;[8] in the latter case, a fixed ξ value of $\pm 0{\cdot}75$ was used for the end nodes. We are therefore presenting the variation of the results with parameter ξ, the element length relative to crack size (L/a) and the computation method used.

The problem was discretized in two different ways depending on whether or not *SQP* elements were employed. In the presence of this type of element, the top left quarter of the sheet was modeled (Model 1 in Figure 3); an internal boundary joining the tips of both cracks was positioned in it and the condition that tractions and displacements should vary quadratically, except in element *SQP*, was imposed. In the absence of *SQP* elements, half of the sheet was modeled (Model 2). The crack was modeled as a function of parameter L/a, L being the length of element *QP* or *SQP*, in such a way that $10, 5, 3$ or 2 elements were used on each edge depending on whether L/a was $0{\cdot}1, 0{\cdot}2, 0{\cdot}3$, or 0·5, respectively; also, the length of elements at the edges was graded in such a way as to avoid abrupt changes. The finest discretization used 60 elements for a quarter sheet and the coarsest only 38.

Figure 4a shows the variation of K_{IN} for the *QP* element in Model 1, which was used exclusively with equations obtained from the hypersingular fundamental solution. Values were plotted in terms of the position of the end nodes NC1 and NC3, given by the ξ coordinate for both, and of the size L of the *QP* and *SQP* elements used. As can be seen, the calculation of the *SIF* from the displacements converged as the discretization decreased, but the degree of convergence varied with the collocation point used in the computations. With NC1, DEU1, the degree of approach depended on ξ; at a ξ value of 0·80 or 0·85, it was virtually independent of element size. With NC2, DEU2, convergence was independent of ξ, however element size influence more the results. The *SIF* values obtained in both cases were quite good (within ± 3 per cent for $L/a \leqslant 0{\cdot}8$).

A similar calculation based on the discretization of Model 2 (Figure 3), with no *SQP* elements and using the hypersingular fundamental solution for one of the crack edges and the usual

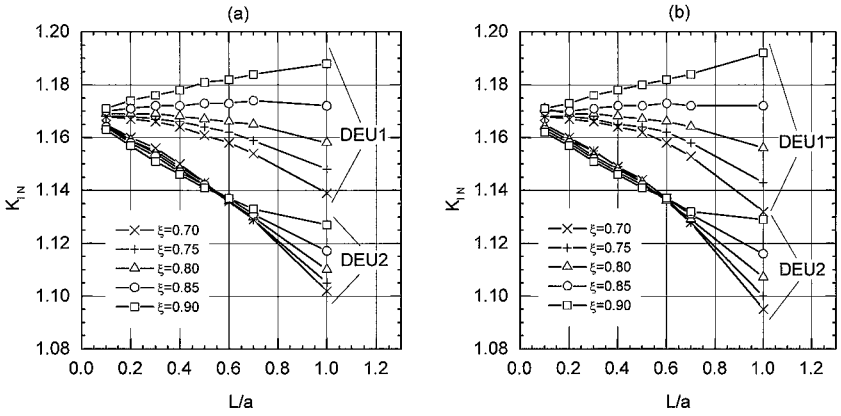

Figure 4. Sheet with two cracks. Variation of the *SIF* with the discretization scheme: (a) Model 1, with *QP* and *SQP*; (b) Model 2, with *QP* only

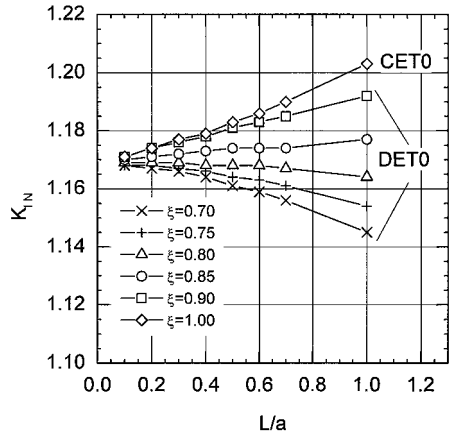

Figure 5. Sheet with two cracks. Variation of the SIF calculated from tractions extrapolated to the crack tip

fundamental solution for the other edge, led to the results shown in Figure 4b. As can be seen, K_{IN} values were very similar to those of Model 1 and also varied similarly, so the previous conclusions are also applicable; the accuracy was similar, so no *SQP* elements were required to ensure good results. Figure 5 shows the variation of the K_{IN} values obtained by extrapolation of the nodal parameters to the crack tip for the *SQP* element (Model 1). As can be seen, K_{IN} values and their changes were similar to those for the values calculated from the displacements at NC1. The graph includes the continuous case, $\xi = 1$, CET0, which provides a comprehensive view of the results; as can be seen, it exhibited the same variation pattern with ξ, and its results were essentially not better than those provided by DEU1 or DET0.

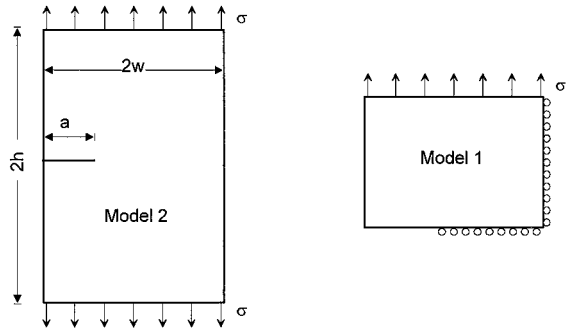

Figure 6. Sheet with a side crack

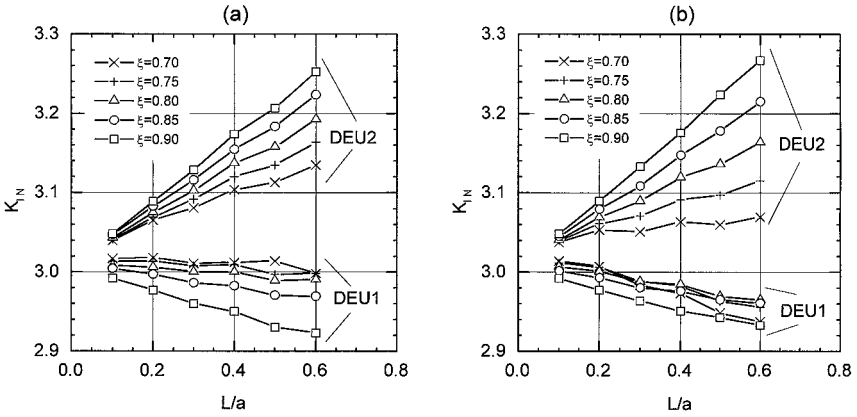

Figure 7. Sheet with a single crack. Variation of the *SIF* with the discretization scheme: (a) Model 1, with *QP* and *SQP*; (b) Model 2, with *QP* only

8.2. Sheet with a side crack. Static SIF

In order to complete the previous study and generalize some conclusions, we carried out a similar parametric study on a sheet containing a side crack (Figure 6). The sheet dimensions were $a = 3$ mm, $w = 3$ mm and $h = 3$ mm; also, the E/σ ratio was 2×10^{11} and the Poisson modulus 0·3. The sheet was discretized similar to those for the previous problem. The reference value used for *SIFs* comparisons was 3·010, Civelek *et al.*[17]

Figure 7a shows the variation of K_{IN} with element size and the position of collocation points NC1 and NC2. Computations were done by using a Model 1 including *QP* and *SQP* elements. As can be seen, the position of extreme collocation points ξ is less important now for the DEU1 results, while the DEU2 curves shows a big influence of this parameter.

A similar effect on the results was observed if a Model 2, including no *SQP* elements, was used, Figure 7b. In this case the DEU1 computations provide cuasi-identical results for *SIFs* that those computed from the *SQP* element by extrapolating the tractions at the crack tip, DET0 in Figure 8. Convergence was good in all instances and the degree to which the different methods

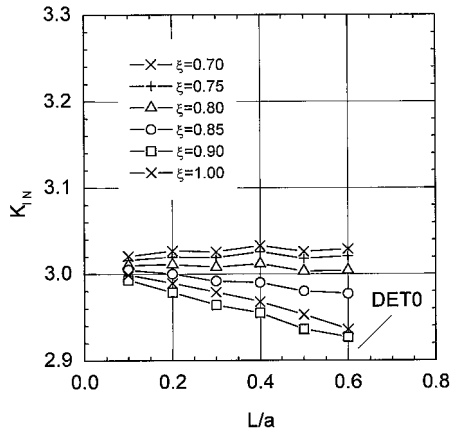

Figure 8. Sheet with a single crack. Variation of the *SIF* calculated from tractions extrapolated to the crack tip

approached the result adopted as reference was dependent on the problem; however, at ξ values about 0·8 and $L/a \leqslant 0{\cdot}4$ all the results were satisfactorily accurate. The most effective methods, however, were those designated DET0 and DEU1, which were similarly precise.

8.3. Diffraction of waves by a crack in an infinite medium. Dynamic SIFs

After the influence of discretization on static problems was investigated, a dynamic problem in the frequency domain was analyzed in order to draw some additional conclusions on its influence and its variation with the frequency.

The problem studied was that of a finite crack in a infinite medium onto which trains of planar waves P or SV impinged (Figure 9) and created incident displacement and stress fields derived from the complex potentials

$$\phi = \phi_0 \exp\left[-\frac{\mathrm{i}\omega}{c_p}(x\cos\gamma + y\,\mathrm{sen}\,\gamma + t\,c_p)\right]; \quad \psi = 0; \quad \mathrm{i} = \sqrt{-1} \tag{73}$$

for P waves and

$$\phi = 0; \quad \psi = \psi_0 \exp\left[-\frac{\mathrm{i}\omega}{c_s}(x\cos\gamma + y\,\mathrm{sen}\,\gamma + t\,c_s)\right] \tag{74}$$

for SV waves, where γ is the incident angle, Figure 9, and ϕ_0 and ψ_0 were calculated in such a way that the normal or tangential stress was unity at the origin.

The diffraction problem was analysed by superimposing the previous incident field with another field consisting of traction distributions at the crack edges of the same magnitude and opposite sign to the incident tractions in such a way that their combination would lead to zero tractions at the edges. The integral representation of tractions and displacements was addressed for the second problem because it was the one that met the conditions for radiation in an infinite space, so only the crack and its surroundings need be discretized.[5]

A half of the discretizations used in the parametric study are shown in Figure 10. As can be seen, case (a) entailed discretizing two semi-infinite boundaries on both sides of the crack;

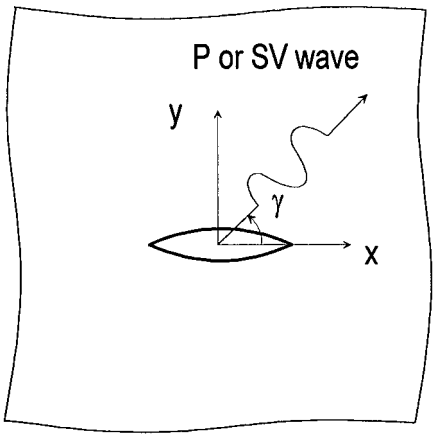

Figure 9. Diffraction of waves by a crack in an infinite medium.

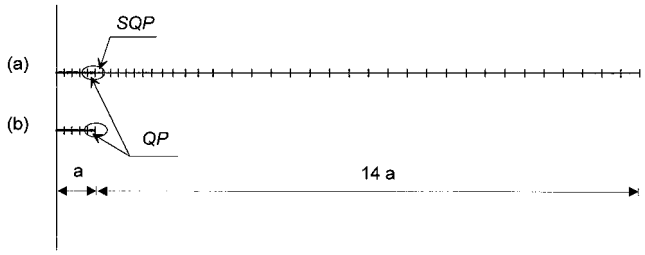

Figure 10. Symmetric half of the discretizations used with a crack in an infinite space: (a) with *QP* and *SQP* elements; (b) mixed method with *QP* alone

however, discretizing a given distance equal to 15 times the crack half-width to simulate half of the problem, and using *QP* and *SQP* elements at the crack tip, were sufficient. This discretization scheme was successfully applied by one of the authors[5] to the same problem however, he used continuous elements rather than the discontinuous elements and hypersingular solution employed here. Figure 10(b) illustrates the latter discretization; only the crack edges were discretized, using the hypersingular solution for one edge and the normal solution for the other (and placing two *QP* element at each tip). In both discretizations, the crack was modeled with 10 elements on each edge (five in each symmetric half), $L/a = 0{\cdot}2$ and $\xi = 0{\cdot}8$ for the end nodes. The infinite boundary was discretized by using an overall 29 elements on each side those of the crack excluded. As can be seen, the number of elements used in discretization (b) was much smaller, and the problem posed by the infinite boundary was circumvented.

Let us first discuss the *SIFs* obtained from the discretization of Figure 10(b), with $v = 0{\cdot}25$, calculated from the displacements of the collocation point lying nearest to the crack, DEU1, at a variable incident angle.

Figure 11 shows for the incidence of *P* waves the *SIF* modulus, normalized by its static value, as a function of the dimensionless frequency $\omega a/c_p$; the results are compared with those reported

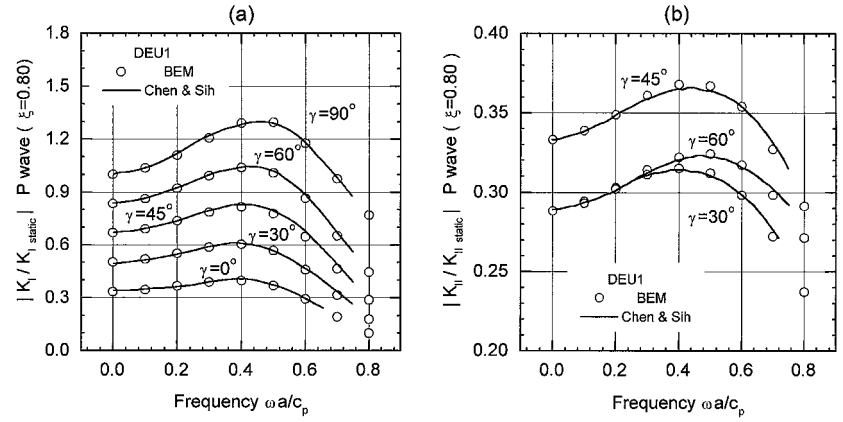

Figure 11. *SIFs* due to the diffraction of *P* waves by a crack in an infinite medium using discretization (b)

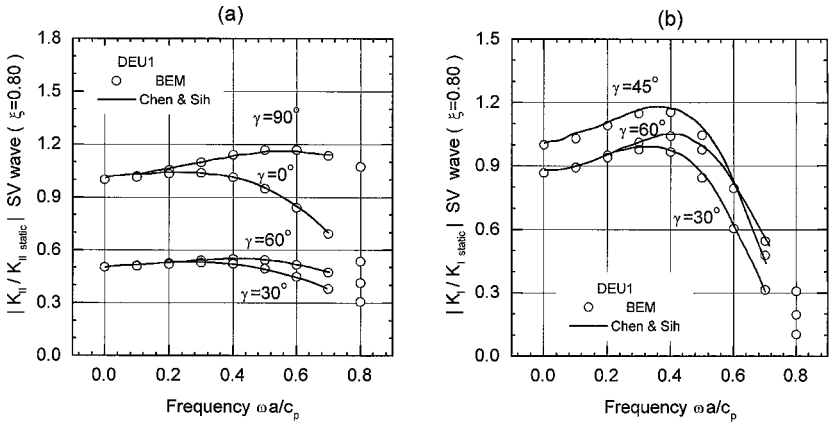

Figure 12. *SIFs* due to the diffraction of *SV* waves by a crack in an infinite medium using discretization (b)

by Chen *et al.*[18] and by Sih *et al.*[19] As can be seen, agreement between the results was very good at all incident angles.

Figure 12 shows the *SIFs* corresponding to the incidence of *SV* waves. The results were also very good, so we may conclude that the discretization used is suited to the problem and the ensuing method accurate enough. In addition, the proposed methodology is more simple and expeditious than earlier computation alternatives.

Once the proposed method was checked to be accurate, its results were compared with those provided by the discretization illustrated in Figure 10(a) and the variation introduced by the *SIF* calculation method at four different ξ values, and a variable dimensionless frequency was analysed.

Table I shows the *SIF* values for the incidence of *P* waves at $\gamma = 90°$ (Figure 9). It compares the results of the two discretizations, three methods (DET0, DEU1 and DEU2) and four positions of NC1 and NC3, all at two different frequencies.

Table I. Incidence of *P* waves. Comparison of the *SIFs* obtained by using different methods, discretization schemes and frequencies

	$\lvert K_I/K_{I\,static}\rvert$ *P*-wave 90°									
$\omega a/c_p$	0·2					0·8				
Discr.	(a)			(b)		(a)			(b)	
ξ	DET0	DEU1	DEU2	DEU1	DEU2	DET0	DEU1	DEU2	DEU1	DEU2
0·75	1·1068	1·1082	1·0990	1·1082	1·0990	0·7714	0·7705	0·7809	0·7705	0·7809
0·80	1·1083	1·1093	1·0978	1·1093	1·0978	0·7692	0·7686	0·7807	0·7686	0·7807
0·85	1·1108	1·1116	1·0968	1·1116	1·0968	0·7661	0·7657	0·7804	0·7657	0·7804
0·90	1·1142	1·1147	1·0952	1·1147	1·0952	0·7625	0·7622	0·7800	0·7622	0·7800

Table II. Incidence of *SV* waves. Comparison of the *SIFs* obtained by using different methods, discretization schemes and frequencies

	$\lvert K_{II}/K_{II\ static}\rvert$ *SV*-wave 90°									
$\omega a/c_p$	0·2					0·8				
Discr.	(a)			(b)		(a)			(b)	
ξ	DET0	DEU1	DEU2	DEU1	DEU2	DET0	DEU1	DEU2	DEU1	DEU2
0·75	1·0520	1·0534	1·0440	1·0534	1·0440	1·0741	1·0739	1·0749	1·0739	1·0749
0·80	1·0536	1·0546	1·0430	1·0546	1·0430	1·0732	1·0730	1·0738	1·0730	1·0738
0·85	1·0560	1·0567	1·0419	1·0567	1·0419	1·0742	1·0740	1·0745	1·0740	1·0745
0·90	1·0595	1·0600	1·0405	1·0600	1·0405	1·0727	1·0725	1·0723	1·0725	1·0723

The tabulated values are given with fourth figures owing by their similarity. A result of the proposed discretization being suitable at every frequency in accordance with the criteria discussed in static problems since the size of the element required to represent the *SIF* properly is usually also sufficient to represent a wide range of frequencies (e.g. with the criterion that there should exist at least four elements per wavelength).

Similar conclusions can be drawn from Table II, which compares the results for the incidence of *SV* waves at 90°. In both cases, methods DET0 and DEU1 provided identical results; those for DEU2 were somewhat different but still very similar.

8.4. Oblique crack in a rectangular sheet. Dynamic SIFs

The last case studied was a dynamic problem with a mixed fracture mode. The Figure 13 shows a sheet with a oblique crack centered in a rectangular sheet. Its inclination angle is 45°, and is loaded dynamically in the axial direction by a uniform traction $p(t) = \sigma \cdot H(t)$, being $H(t)$ the Heaviside step function starting at $t = 0$. This problem was selected from the paper of Murti *et al.*,[20] where is analysed by *FEM*. The sheet and crack dimensions were: $h = 30$ mm, $w = 30$ mm,

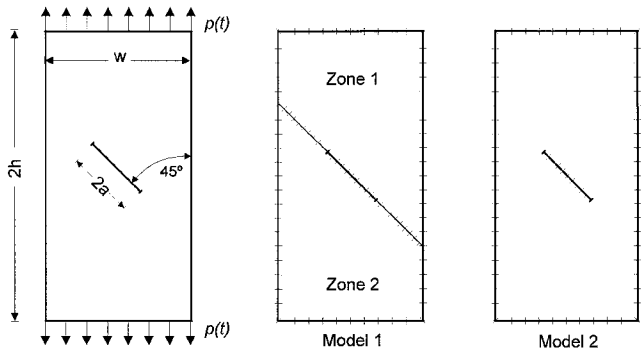

Figure 13. Oblique crack in a rectangular sheet. Models and discretizations

$a = 5\sqrt{2}$ mm, and the material properties assumed were: $\upsilon = 0{\cdot}3$, $\mu = 76{\cdot}923$ GPa, $\rho = 5000\,\mathrm{kg/m^3}$, and internal damping of 2 per cent (damping factor $\beta = 0{\cdot}02$).

This damping in the frequency domain formulation is taken in account using a complex shear modulus $\hat{\mu} = \mu(1 + \mathrm{i}2\beta)$, and complex wave speeds. The inclusion of this hysteretic damping stabilizes the transient response obtained from the *Fast Fourier Transform* algorithm, *FFT*, in its application to the product of the frequency domain results times the frequency transform of the Heaviside step function. The introduction of a small amount of internal damping is an alternative to the use of a filter before the *FFT* inversion, but has the problem that reduces the peak amplitudes.

The analysis was carried out with two different models. The Model 1 has two zones that are coupled using the compatibility and equilibrium equations along the common boundary. All the boundaries of this model were discretized with discontinuous elements, disposing ten of them on the crack length, Figure 13. *Stress Intensity Factors* values in this model were computed from the nodal parameters of the *SQP* and *QP* elements at the crack tip (DET0, DEU1, and DEU2 approximations).

The second model utilized was Model 2, Figure 13. In this model, with only a zone, the crack edges were discretized using the hypersingular solution for one edge and the normal solution for the other, using four *QP* discontinuous elements, two in each crack tip. The displacements of the collocation points of these *QP* elements were used to obtain the *SIFs* (DEU1 and DEU2 approximation). In both models the position of the extreme collocation points in all the discontinuous elements was $\xi = \pm 0{\cdot}8$, including the *QP* and *SQP* elements.

The results obtained in the frequency domain for the *SIFs* of modes I and II, computed with the approximations DET0, DEU1 and DEU2, were similar for the two models. Because this similarity only the results obtained with the Model 2, mixed method, and DEU1 approximation, were showed.

The Figure 14, shows the evolution of the real and imaginary part of the mode I and mode II *SIFs*, normalized by $\sigma\sqrt{a\pi}$, with the dimensionless frequency $\omega a/c_s$. The peaks are not infinite because the damping, and they mark the resonance frequencies of the cracked sheet.

In Figure 15, the transient evolution of the normalized *SIFs* of mode I and mode II, are plotted and compared with the results obtained by Murti *et al.*[20] The agreement between both solutions is good enough, showing that the proposed method is a valid alternative to the existing tools for analyze mixed mode problems in finite sheets.

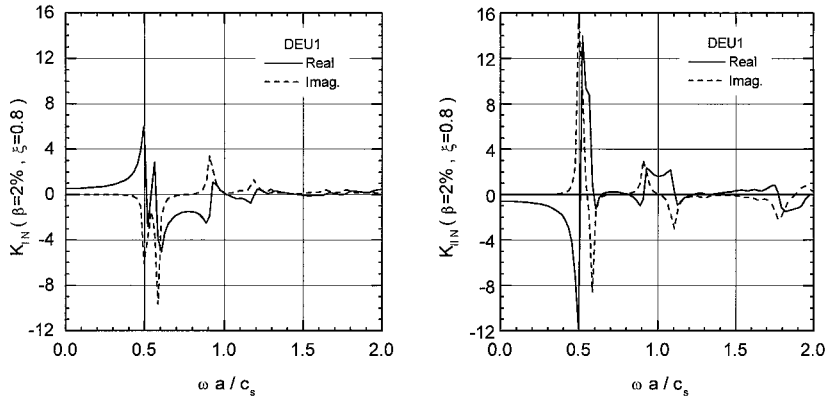

Figure 14. Real and imaginary parts of the normalized *SIFs* for a sheet with an oblique crack

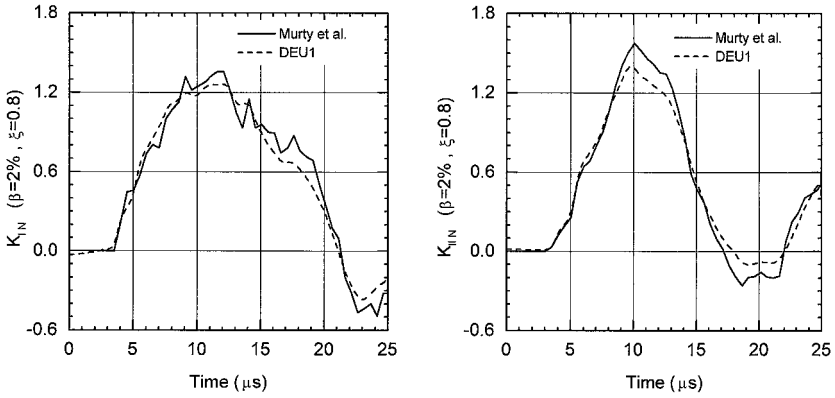

Figure 15. Transient *SIFs* for a sheet with an oblique crack under a step traction

9. CONCLUSIONS

This paper presents the expressions for the hypersingular nuclei used in the integral representation of tractions in the *Boundary Element Method* as applied to dynamic problems in the frequency domain and analyses their splitting into their singular and non-singular parts, which facilitates their numerical treatment and the potential use of advanced integration techniques. This formulation was used to develop computer software based on discontinuous quadratic elements that enables the analysis of static and dynamic fracture problems.

We also developed a discontinuous *Singular-Quarter-Point* element, very useful for computing *Stress Intensity Factors* of cracks, which had never been used to date. The element is of a high interest, particularly for addressing problems involving interfaces coinciding with the crack tip.

The proposed formulation was used in parametric studies that revealed the flexibility and computational power of the ensuing approach, as well as the suitability of the *Mixed Boundary Element Method* for calculating static and dynamic *SIFs*.

The static parametric studies performed revealed that the use of discontinuous elements does not detract from precision, providing excellent results for *SIFs* whether they are calculated from the displacements of the collocation points, *QP* elements, or from traction values extrapolated to the crack tip in *SQP* elements.

Regarding discretization size, the results revealed that a *QP* or *SQP* element size equal to or less than 0·4 times the crack dimension and end collocation points, NC1 and NC3, between $\xi = 0{\cdot}75$ and 0·90 provide excellent results with all the *SIF* computation methods employed.

Applications to dynamic problems revealed that the static discretizations needed to calculate *SIFs* are sufficient for the analysis over a wide frequency range and that no additional mesh refining is required in most cases. Specifically, the results for the diffraction of *P* and *SV* waves by a crack in an infinite space, and for a oblique crack in a finite sheet, mixed mode, were compared favourably with those previously obtained by other authors for similar problems.

In conclusion, the proposed hypersingular formulation is a highly powerful numerical tool for studying Fracture Mechanics problems, especially in combination with the traditional formulation for modelling the two geometrically coincident edges of a crack, without the need to introduce non-existing internal boundaries.

ACKNOWLEDGEMENTS

Partial funding of the investigations that led to the above results and conclusions by Spain's DGICYT in the framework of Projects PB 93-1184 and PB 93-1191 is gratefully acknowledged.

REFERENCES

1. J. Dominguez, *Boundary Elements in Dynamics*, Computational Mechanical Publications and Elsevier, Amsterdam, 1993.
2. M. H. Aliabadi and D. P. Rooke, *Numerical Fracture Mechanics*, Computational Mechanics Publications and Kluwer Academic Publishers, Dordrecht, 1991.
3. M. H. Aliabadi, C. A. Brebbia and V. Z. Parton (eds), *Static and Dynamic Fracture Mechanics*, Computational Mechanics Publications, Southampton, 1994.
4. J. Martinez and J. Dominguez, 'On the use of quarter-point boundary elements for stress intensity factor computations', *Int. J. Numer. Meth. Engng.*, **20,** 1941–1950 (1984).
5. F. Chirino and J. Dominguez, 'Dynamic analysis of cracks using boundary element method', *Engng. Fract. Mech.*, **34,** 1051–1061 (1989).
6. J. Dominguez and R. Gallego, 'Time domain boundary element method for dynamic stress intensity factor computations', *Int. J. Numer. Meth. Engng*., **33,** 635–647 (1992).
7. F. Chirino, R. Gallego, A. Sáez and J. Dominguez, 'A comparative study of three boundary element approaches to transient dynamic crack problems', *Engng. Anal. Bound. Elem*., **13,** 11–19 (1994).
8. A. Saez, R. Gallego and J. Dominguez, 'Hypersingular quarter-point boundary elements for crack problems', *Int. J. Numer. Meth. Engng.*, **38,** 1681–1701 (1995).
9. A. Portela, M. H. Aliabadi and D. P. Rooke, 'The dual boundary element method: effective implementation for crack problems', *Int. J. Numer. Meth. Engng.*, **33** (6) 1269–1287 (1993).
10. P. Fedelinski, M. H. Aliabadi and D. P. Rooke, 'A single-region time domain BEM for dynamic cracks problems', *Int. J. Solids Struct.*, **32** (24) 3555–3571 (1995).
11. P. Fedelinski, M. H. Aliabadi and D. P. Rooke, 'The Laplace transform DBEM for mixed-mode dynamic analysis', *Comput. Struct.*, **59** (6) 1021–1031 (1996).
12. M. L. Williams, 'Stress singularities resulting from various boundary conditions in angular corners of plates in extension', *J. Appl. Mech. ASME*, **19,** 526–528 (1952).
13. G. R. Irwin, 'Analysis of stresses and strains near the end of a crack traversing plate', *J. Appl. Mech. ASME*, **24,** 361–364 (1957).
14. G. E. Blandford, A. R. Ingraffea and J. A. Liggett, 'Two-dimensional stress intensity factor computations using the boundary element method', *Int. J. Numer. Meth. Engng*., **17,** 387–404 (1981).

15. Y. Murakami (ed.), *Stress Intensity Factors Handbook*, Vol. 1, Committee on Fracture Mechanics SMS Japan, Pergamon Press, Oxford, 1987.
16. H. Nisitani, 'Tension of a strip with symmetric edge cracks or elliptical notches', *Trans. Japan Soc. Mech. Engng.*, **49**-349, 2518–2526 (1975).
17. M. B. Civelek and F. Erdogan, 'Crack problems for a rectangular sheet and a infinite strip', *Int. J. Fract*., **19,** 139–159 (1982).
18. E. P. Chen and G. C. Sih, 'Scattering waves about stationary and moving cracks', in G. C. Sih (ed.), *Mechanics of Fracture* 4: *Elastodynamic Crack Problems*, Chap. 3, *Noordhoff*, Leiden, 1977.
19. G. C. Sih and J. F. Loeber, 'Wave propagations in a elastic solid with a line of discontinuity or finite crack', *Quart. Appl. Math.*, **27,** 193–213 (1969).
20. V. Murti and S. Valliappan, 'The use of quarter-point element in dynamic crack analysis', *Engng. Fract. Mech.*, **23,** 585–614 (1986).

